Materials and Design 65 (2015) 127–138

Contents lists available at ScienceDirect

Materials and Design

journal homepage: www.elsevier.com/locate/matdes

Technical Report

A bottom-up approach for optimization of friction stir processing parameters; a study on aluminium 2024-T3 alloy

Naresh Nadammal [a,*], Satish V. Kailas [a], Satyam Suwas [b]

[a] Department of Mechanical Engineering, Indian Institute of Science, Bangalore, India
[b] Department of Materials Engineering, Indian Institute of Science, Bangalore, India

ARTICLE INFO

Article history:
Received 19 July 2014
Accepted 3 September 2014
Available online 16 September 2014

ABSTRACT

Friction stir processing (FSP) is emerging as one of the most competent severe plastic deformation (SPD) method for producing bulk ultra-fine grained materials with improved properties. Optimizing the process parameters for a defect free process is one of the challenging aspects of FSP to mark its commercial use. For the commercial aluminium alloy 2024-T3 plate of 6 mm thickness, a bottom-up approach has been attempted to optimize major independent parameters of the process such as plunge depth, tool rotation speed and traverse speed. Tensile properties of the optimum friction stir processed sample were correlated with the microstructural characterization done using Scanning Electron Microscope (SEM) and Electron Back-Scattered Diffraction (EBSD). Optimum parameters from the bottom-up approach have led to a defect free FSP having a maximum strength of 93% the base material strength. Micro tensile testing of the samples taken from the center of processed zone has shown an increased strength of 1.3 times the base material. Measured maximum longitudinal residual stress on the processed surface was only 30 MPa which was attributed to the solid state nature of FSP. Microstructural observation reveals significant grain refinement with less variation in the grain size across the thickness and a large amount of grain boundary precipitation compared to the base metal. The proposed experimental bottom-up approach can be applied as an effective method for optimizing parameters during FSP of aluminium alloys, which is otherwise difficult through analytical methods due to the complex interactions between work-piece, tool and process parameters. Precipitation mechanisms during FSP were responsible for the fine grained microstructure in the nugget zone that provided better mechanical properties than the base metal.

1. Introduction

Metal working techniques that enhance localized mechanical properties of a material is getting much importance nowaday due to specific application requirements. Localized microstructural modification and mechanical property enhancement techniques that do not alter the properties of other regions in a material are the most important among these metal working operations.

Friction stir processing (FSP) is a severe plastic deformation (SPD) technique introduced by Mishra et al. [1]. The process is derived from basic principles of friction stir welding (FSW), a solid state metal joining technique developed at TWI (The Welding Institute) U.K. in 1991. The joining/welding process involves traversing of a non-consumable rotating tool with a shoulder and a pin along the interface between two work pieces, whereas for FSP, the tool is traversed along the selected region in the specimen which is to be modified. Though the process seems simple, as per the above description, a number of processing parameters makes the optimization of FSP a difficult task.

Major processing parameters of FSP are the vertical pressure on tool (plunge depth given in the workpiece), tool rotational speed, tool traverse speed, tool tilt angle and the tool geometry. If the process parameters are not optimum, then a defect in the form of a through hole is observed in friction stir processed materials, and this defect is commonly referred to as wormhole defect. Though few other defects are also observed in FSW/FSP, significance of those defects are lesser compared to the wormhole defect [2]. Hence optimizing the process parameters before performing any detailed microstructural study is an important aspect to be followed in FSP. But in many of the previous studies on FSP [3–5] this practice has not been observed to be followed and the correlation of microstructure to property can be less relevant in such cases.

Most of the optimization work on FSW/FSP has been done using computational and analytical methods or a combination of both experimental and numerical methods, such as Taguchi technique

* Corresponding author. Tel.: +91 9538220749.
E-mail address: nareshnn@mecheng.iisc.ernet.in (N. Nadammal).

http://dx.doi.org/10.1016/j.matdes.2014.09.005
0261-3069/

[6,7]. Some of the other optimization works were carried out using methods such as gradient technique [8] and artificial neural network [9]. As with the limitations exerted by constraints in numerical modeling, it is difficult to achieve the exact processing conditions as in actual experiments for a process like FSP, which involves complex thermo-mechanical interactions. Hence, a systematic experimental procedure for the optimization of process parameters is at par the best suitable option for a process like FSP.

By considering all the above aspects, a bottom-up approach has been attempted for the optimization of processing parameters for FSP of aluminium alloy 2024-T3. The starting tool geometry is taken as the cylindrical tapered tool pin with a flat shoulder, which is simplest of all the geometries that can be considered for an FSP. Tool tilt angle is kept constant at 2°. The other three parameters plunge depth; tool rotation speed and tool traverse speed were optimized through a bottom-up approach and explained detail in the experimental section.

In most of the FSW/FSP literature this optimization procedure has not been found to be followed. Hence, in the current work, FSP performed with the optimum parameters is characterized in detail using advanced characterization methods. Residual stress measurement is one of the most important aspects to be considered in any metal working operation, especially when heat generation is associated with it. In FSP, during the process, major work input is the heat generated by friction between the tool shoulder and workpiece material. Once the process starts, plastic deformation also contributes to generating significant heat. Hence, the measurement of residual stress is much important in projecting FSP as a commercially viable technique for the bulk production of ultrafine grained materials.

The flow of work in current study can be summarized as follow: a systematic experimental bottom-up approach has been developed for optimizing the process parameters for FSP of AA 2024-T3. Bulk and micro tensile testing has been done on the optimum processed sample. The optimum processed sample has been characterized in detail using SEM and EBSD. Residual stress was measured on the optimum processed surface using X-ray diffraction.

2. Experimental details

2.1. Materials and machine

A heat treatable aluminium alloy 2024 in T3 tempered condition with a plate thickness of 6 mm was selected as the working material for FSP. Elemental composition of the alloy was determined using Wavelength Dispersive Spectroscopy (WDS) technique on a JEOL Electron Probe Micro Analyzer (EPMA). Elemental composition of the alloy is given in Table 1. Tool material used for FSP was made from Hot Die Steel (HDS) in H13 hardened condition. After machining to the specific geometry, the tool is case hardened. The tool shoulder diameter selected was 20 mm, which was chamfered from a 25 mm diameter cylinder. Tool pin shape is that of a frustum of a cone with a tapered diameter of 6 mm at the top to 4 mm in the bottom for a length of 5.4 mm.

A custom designed machine with tool in a horizontal position and the specimen held in vertical position was developed with the help of ETA technologies, Bangalore, India. The machine has the capability to vary the tool RPM, traverse speed and plunge depth during a process.

Table 1
Elemental composition of the alloy 2024-T3.

Al	Cu	Mg	Mn	Si	Zn
94.8	3.6	1.45	0.45	0.06	0.05

2.2. Optimization experiments

The tool tilt angle was kept constant at 2°. Three other parameters, plunge depth in the specimen, tool rotational speed and tool traverse speed, were optimized. Among these three parameters, order of parameter optimization was selected after a number of trial experiments with these parameter combinations. Selected order from these experiments was (1) plunge depth (2) rotational speed and (3) traverse speed.

Tensile and microstructural specimens were cut from the various friction stir processed specimens. The way in which the specimens were cut is shown in Fig. 1, for the varying plunge depth experiments. Optical imaging of the transverse cross section of the specimens were done using Metallovert Carl Zeiss optical microscope. Tensile testing of the samples were done using an Instron 8032 servo hydraulic UTM. Scanning Electron Microscopy (SEM) and Electron Back-Scattered Diffraction (EBSD) was done on an ESEM Quanta microscope (Quanta 200, FEI) with tungsten filament as the source for generating electrons.

2.2.1. Varying plunge depth experiment

Tool rotation rate and traverse speed were kept constant at 500 RPM and 25 mm/min respectively. Plunge depth was varied from 5.00 mm to 5.8 mm for a processing distance of 200 mm and a tool pin length of 5.4 mm. For each 20 mm of FSP region, a tensile and micro structural specimen was taken, as shown in Fig. 1. Optimum plunge depth was selected by correlating the ultimate tensile strength and observing the macrograph taken for each sample.

2.2.2. Varying RPM experiment

With the obtained optimum plunge depth of 5.63 mm from the above set of varying plunge depth experiments and keeping the same constant traverse speed, tool rotational rate was varied from 200 to 1600 RPM. This was done in two steps – in the first step RPM was varied from 200 to 900 and in the next from 900 to 1600.

2.2.3. Varying traverse speed experiment

With the obtained optimum plunge depth and rotational speed from above two experiments traverse speed was varied from 10 to 170 mm/min. Here too the experiment was done in two steps – in the first stage by varying traverse speed from 10 to 90 mm/min, and in the next by varying from 90 to 170 mm/min.

2.2.4. Optimum FSP experiment with the optimum processing parameters

The optimum process parameters were selected from the above experiments and an optimum FSP has been done.

2.3. Mechanical property evaluation

Bulk tensile testing was done on an Instron 8032 servo hydraulic UTM at a strain rate of 10^{-3} s^{-1} and for a specimen gauge length of 60 mm. In the case of varying plunge depth experiments, thickness of the tensile specimen was varied from 5.4 to 5.8 mm based on the depth of processing. This was done with the help of microstructural specimen taken from a near region. It is to avoid the effect of unprocessed region at the bottom while testing. In all the other cases, an equivalent thickness of approximately 0.2–0.3 mm from the bottom was removed based on the optimum plunge depth value obtained. Hence, approximate thickness of the specimen was within the range of 5.6–5.7 mm. Exact dimensions were measured for each specimen at different regions along the gauge length and the average value was used for calculating tensile properties. Specimen geometry is shown in Fig. 2.

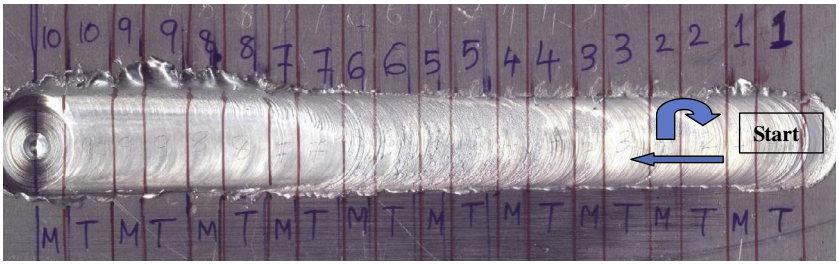

Fig. 1. Varying plunge depth experiment done on AA 2024-T3. Whole specimen size is 250 * 140 * 6 mm. 'M' stands for microstructural specimen and 'T' for tensile specimen.

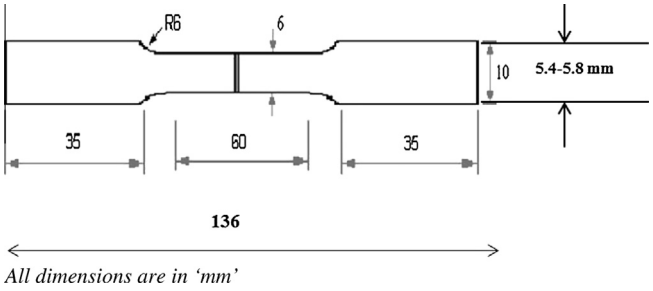

Fig. 2. Specimen geometry used for bulk tensile testing. All dimensions are in 'mm'. As per ASTM: E8 standard.

Micro-tensile testing was done on a Zwick/Roell screw driven Universal Testing Machine (UTM) for a strain rate of $10^{-3}\,s^{-1}$ and a specimen gauge length of 6 mm. The specimen dimensions are given in Fig. 3a. Specimens were taken from the top, bottom and middle of the nugget zone of optimum FSP samples by dividing the whole thickness into 3 slices of 2 mm each as shown in Fig. 3b. These specimens were fine polished on both sides to remove the discontinuities present on their surface and the final thickness of micro-tensile specimens was approximately 1.8 mm. Specimens were prepared through conventional machining operations.

2.4. Residual stress measurements

Residual stress measurement specimen having a dimension of 30 mm * 25 mm * 6 mm was prepared from the region close to the exit pin hole. Sectioning of the specimen was done using a low speed band saw and cold water as lubricant. Sectioning through exit pin hole allows easy cutting without having any effect on the processed region. On the other end, cutting was done after 30 mm and the stress was measured on the surface close to the remnant of exit pin hole. Thus, any effect of stress relaxation during sectioning was avoided. The average residual stress at the surface of the optimum FSP sample was measured using a Bruker D8 Discover X-ray diffractometer with a one dimensional detector. Source X-ray used was Cu having a $K\alpha_1$ wavelength of 1.540562 Å and $K\alpha_2$ wavelength of 1.544390 Å. The (220) peak of FCC aluminium was selected for measuring the residual stress on the processed surface of the sample. Analysis of residual stress was done using the Leptos software developed by Bruker AXS GmbH [10].

2.5. Microstructural observations

Transverse cross section of the optimum processed samples were polished using SiC papers with decreasing particle sizes up to a SiC grade of P3000. Cloth polishing was followed with diamond particles of 3 μm and 0.25 μm respectively, and kerosene as lubricant. Samples were etched using Keller's reagent. Microstructural observations were made using a Metallovert Carl Zeiss optical microscope and FEI ESEM Quanta 200 Scanning Electron Microscope (SEM). Microstructure of the base metal was taken and compared with the processed sample. For the FSP sample, top, middle and bottom of nugget zone across the thickness and the advancing and retreating sides were also observed.

Electropolishing was done before doing EBSD on the processed samples, this is required to remove strain present on the polished surface and for obtaining better results while characterize using EBSD. Standard A2 electrolyte was used with a voltage of 26 V and a time period of 25 s. EBSD facility available in the same SEM was used.

3. Results

3.1. Varying plunge depth experiment

Variation of ultimate tensile strength with the plunge depth is shown in Fig. 4. In the first three cases, reason for lower values of UTS is the insufficient plunge depth leading to an insufficient filling of the processed zone as the tool traverses. A considerable drop of UTS value was observed for the second sample compared to the first. This may be due to the fact that for the first sample a portion of the base metal is a part of it, and the proper plunging starts only from the second specimen onwards. UTS value increases gradually but not more than base material strength at any plunge depth, and decreases as the plunge depth increases to

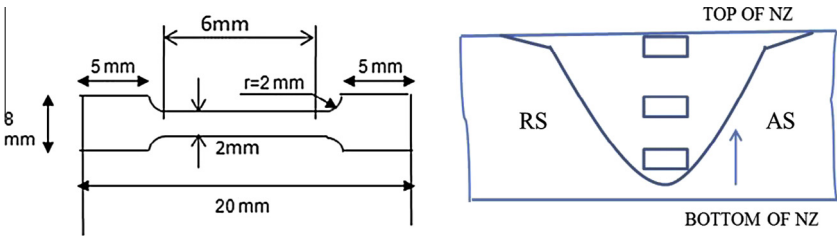

Fig. 3. (a) Specimen geometry used for micro tensile testing. Not as per ASTM standard. (b) Transverse cross section showing the positions at which samples were taken for micro-tensile testing.

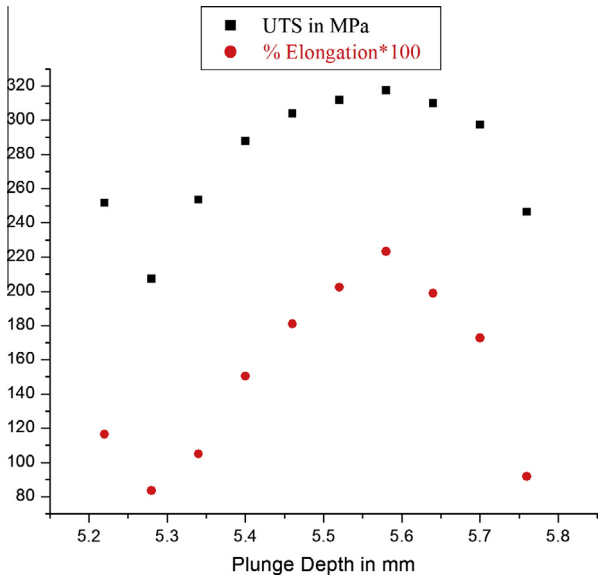

Fig. 4. Variation of UTS in MPa and % elongation with the plunge depth in mm. Percentage elongation is multiplied with 100 in the graph for scaling.

more than 0.3 mm of shoulder penetration into the work piece material. It can be observed from the figure that the variation of the UTS and percentage elongation follows the same trend. This trend confirms the fact that combination of strength and ductility is possible for a friction stir processed aluminium alloy.

UTS and percentage elongation values were almost same for plunge depth values in the range of 5.55–5.75 mm. Hence, a varying plunge depth experiment was conducted again within this particular range, i.e., from 5.5 to 5.7 mm. Variation of ultimate tensile strength for this plunge depth range is plotted in Fig. 5. It can also be seen from the plot that the variation in this narrow range also follows the same trend as UTS, and percentage elongation followed in the wide range as in the previous experiment. This fact again confirms the strength, ductility combination of the materials prepared with FSP.

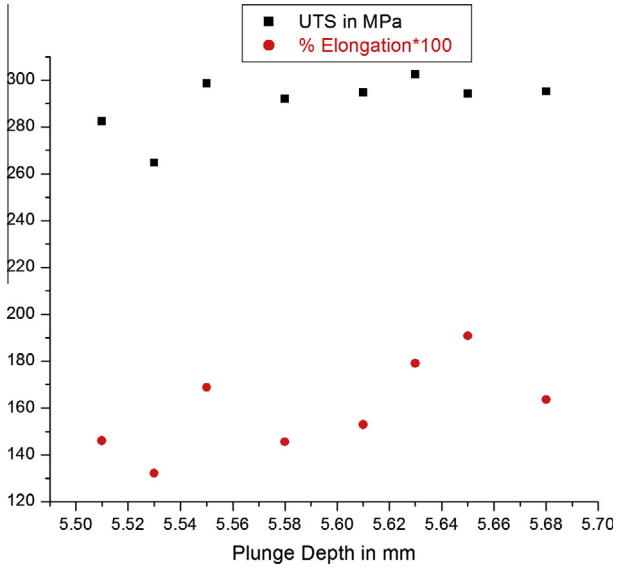

Fig. 5. UTS and percentage elongation Vs Plunge depth for the second set of varying plunge depth experiment. Percentage elongation is multiplied with 100 in the graph for scaling.

From Fig. 5 it can be seen that the maximum UTS value is obtained for a plunge depth of 5.63 mm. This value has been selected as the optimum plunge depth for FSP of this particular alloy as per the other fixed boundary and experimental conditions. The corresponding macrograph is also shown in Fig. 6. Advancing side, which is the defect prone region, does not have any visible wormhole defect, but it does have a sharp boundary associated with it and being a region of discontinuity, fracture can occur along this boundary.

3.2. Varying RPM experiment

Variation of UTS and percentage elongation with the tool rotational speed (RPM) is shown in Fig. 7. It is observed from the figure that as the RPM increases the values of both UTS and percentage elongation follows the same pattern. Their values decrease as the RPM increase. Experiments done at higher RPM produced defective FSP, and hence the UTS and ductility values were very low. Maximum value of UTS and percentage elongation is observed in the case of lower RPM in the range of 200–400 for this particular alloy, keeping other boundary conditions intact.

Two specimens had almost the same value of UTS, whereas the ductility for the second specimen was comparatively lower than the first. Among these, the higher RPM was selected as the optimum for this particular alloy for the previously optimized plunge depth. Hence, 350 RPM has been selected as the optimum RPM from the varying RPM experiments. Macrograph of the processed region with the optimum plunge depth of 5.63 mm and the optimum RPM 350 is shown in Fig. 8.

3.3. Varying traverse speed experiment

The variation of UTS and percentage elongation with the traverse speed is shown in Fig. 9. It can be observed from the plot that a large variation of UTS and ductility is observed with the variation in traverse speed. A higher value of strength and ductility is observed at the start of the experiment for a very low traverse speed. But as per the practical aspects are concerned, this traverse speed is very low for a material like aluminium used in structural applications. A higher value of UTS and percentage elongation was again observed for a traverse speed of 95 mm/min. UTS value was 350 MPa and the elongation of 2.3%. Hence, the optimum traverse speed selected was 95 mm/min for a plunge depth of 5.63 mm and 350 RPM.

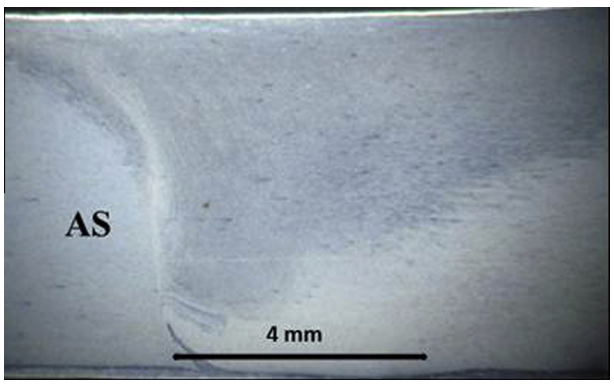

Fig. 6. Macrograph of the sample corresponding to a plunge depth 5.63 mm from varying plunge depth experiment 2.

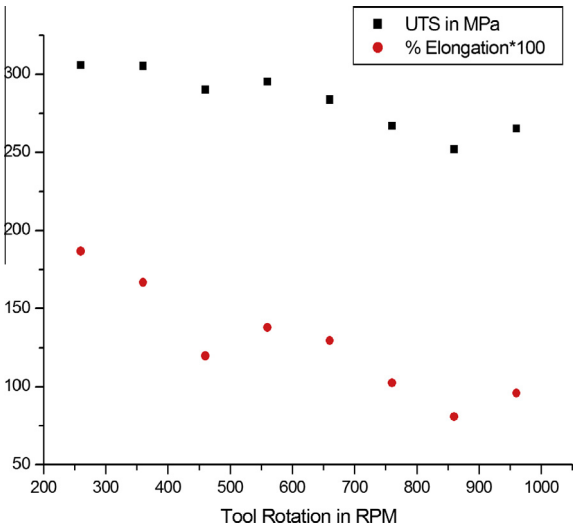

Fig. 7. Variation of UTS and percentage elongation with RPM. Percentage elongation is multiplied with 100 for scaling.

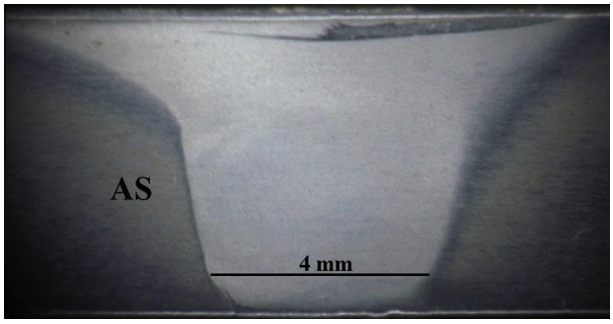

Fig. 8. Transverse cross section image for FSP done at 5.63 mm plunge depth and 350 RPM.

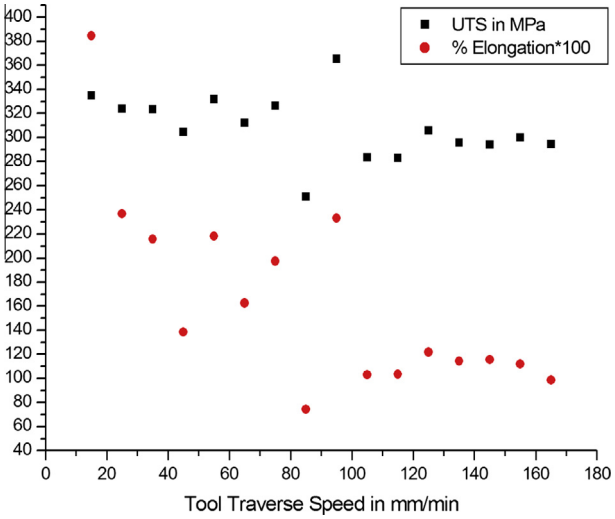

Fig. 9. Variation of UTS and percentage elongation with traverse speed. Percentage elongation is multiplied with 100 for scaling.

3.4. Optimum parameters FSP

The optimum parameters selected were a plunge depth of 5.63 mm, RPM of 350 and a traverse speed of 95 mm/min. Optimum FSP was achieved with the cylindrical tapered tool used in optimizing the parameters, the transverse cross section of the sample is shown in Fig. 10a. This also shows a small discontinuity at advancing side in the form of a sharp boundary. In most of the previous work done on FSW/FSP of aluminium alloys, tools with other complex geometries were used. A threaded tapered tool pin is the very next possible tool geometry from a cylindrical tapered tool. Threaded tool has been tried with the same pin length, all other tool parameters remaining the same. This is because a threaded tool allows vertical mixing of the material in a much better way, and hence can avoid the sharp boundary and other discontinuities in the advancing side. This produced a much better processed region and avoided the discontinuity in the boundary. SEM image of the advancing side of the sample processed with threaded tool is shown in Fig. 10 b. From these results the optimum FSP sample is selected as the one that was processed with the threaded tool geometry and using the optimum process parameters.

3.5. Mechanical properties

Comparison of base metal strength and the optimum single pass FSP samples was made as shown in Fig. 11. FSP sample was made in such a way that the processed region comes in the gauge length along with a small portion of base metal. The 0.2% yield strength, ultimate tensile strength and the percentage elongation (which is multiplied by 50 to scale up and match the values of yield strength and ultimate tensile strength) are compared in the figure.

It is clear from the plot that the 0.2% yield strength and the ultimate strength of the base metal and the single pass FSP sample are almost the same. It is also observed that ductility of the optimum FSP sample is also almost same as that of the base metal. These observations are interesting in a way that a single pass optimum FSP sample microstructure is a mix-up of heterogeneous regions such as the nugget zone, TMAZ, HAZ, base metal and the boundary between these regions. Property of this sample is compared with that of the homogenous base metal structure.

Micro tensile testing results are shown in Fig. 12. Samples were taken across through thickness of the nugget zone so as to have a check on the homogeneity of microstructure.

It has been observed that for all the specimens ultimate tensile strength values are higher than 500 MPa, which is higher than the base metal strength of 450 MPa. Percentage elongation of the processed samples are also higher than that of the base metal. This is the major strength of friction stir processing in which the strength and ductility of a material is balanced and its more than the base materials strength in the processed region. It is noteworthy from Fig. 12 that the percentage elongation is multiplied by 10 and not 100 as in the case of optimization experiments. It is also to be noted that the gauge length is only 6 mm in the case of microtensile testing, and hence a smaller increase in gauge length will correspond to a higher ductility. But here in this study obtained ductility values are one order of magnitude higher than the base metal values. So the effect of a smaller gauge length do not have much significance here.

3.6. Residual stress

Residual stress was measured on the surface of optimum friction stir processed sample. To estimate the residual stress, stress-free d spacing of the alloy 2024 was required. This was done by annealing the base metal at 500 °C for 3 h in a tube furnace. The d spacing value corresponding to the 2θ value of (220) peak of the annealed sample was taken as the standard d value. Variation of strain with $\mathrm{Sin}^2\psi$ is also shown in Fig. 13, exhibiting the general ψ splitting behavior for the obtained residual stress. This happens

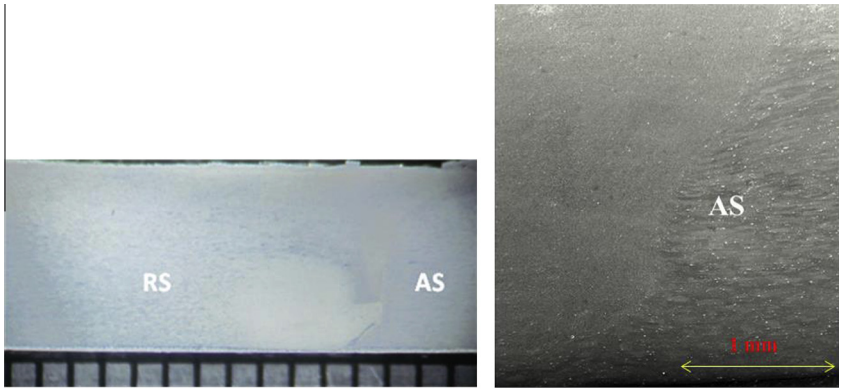

Fig. 10. (a) Transverse cross section of optimum FSP done with cylindrical tapered tool geometry, and (b) SEM Image of the optimum friction stir process done with threaded tool geometry. The region at the advancing side where a sharp boundary was created during optimum FSP with cylindrical tapered tool geometry, is highlighted.

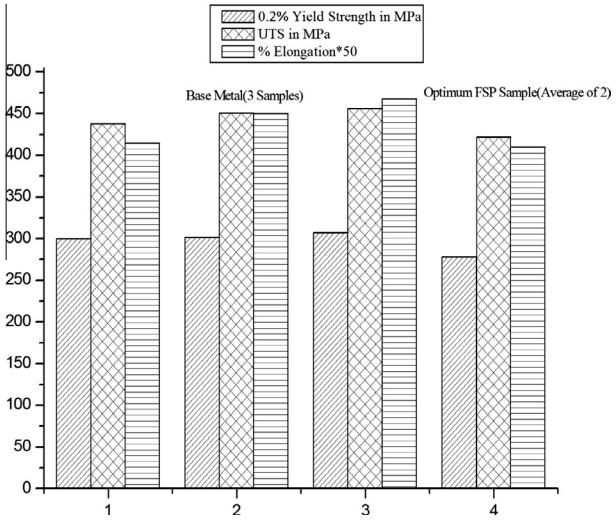

Fig. 11. Mechanical properties comparison of base metal and optimum friction stir processed samples. Percentage elongation is multiplied with 50.

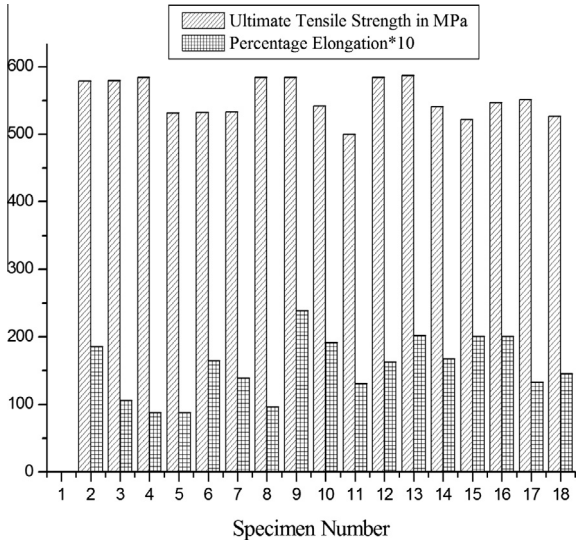

Fig. 12. Microtensile testing results. Percentage elongation is multiplied with 10.

because of the non-homogenous stress distribution present in the processed samples.

For peak evaluation method gravity based on center of gravity of the diffraction line, stress along the processing direction, or the longitudinal stress was tensile in nature with a magnitude of 12.4 ± 12.4 MPa. With sliding gravity method [11] on the other hand, the obtained longitudinal stress was of tensile in nature with a magnitude of 25.4 ± 15.3 MPa. For the most common Pearson VII method of peak fitting, the obtained value of longitudinal stress was tensile, with a magnitude of 13.1 ± 11.6 MPa. Measured residual stress in the transverse direction was negligible compared to the values in longitudinal direction. All the values of the normal residual stress obtained were much lesser than the base material yield strength of 290 MPa.

4. Discussions

4.1. Optimization of process parameters for AA 2024-T3

Though the basic feature of the process seems to be simple there are complex thermo-mechanical interactions associated with FSP. Hence optimizing the process parameters is a difficult task, and much of the previous work on FSP was carried out in trial and error format to optimize the processing parameters. In this paper a bottom-up approach was attempted for optimizing the processing parameters for heat treatable aluminium alloy 2024-T3. It was observed from the whole optimization process that a combination of the three major processing parameters gives a defect free FSP with a minimum sharp boundary between the processed region and the base material. This sharp boundary can always act as a weaker region for stress concentration during any further straining of the processed sample, as in mechanical testing. In other cases, though the defects were not present a sharp boundary was observed on the advancing side of the processed zone. This is due to the large strain gradient experienced on the advancing side of FSP samples, which is inherent with the basic nature associated to the geometries and movement of work piece and tool during FSP. Hence the presence of this sharp boundary should be avoided at any cost for a successful FSP as it can have adverse effect on the fatigue performance of friction stir processed components [12].

In most of the past investigations the major parameters optimized were the tool rotation speed and the tool traverse speed. Detailed work on the parameter plunge depth or normal load is available from the work of Kumar and Kailas [13]. In their work FSP was done in feed control mode by keeping the backing plate

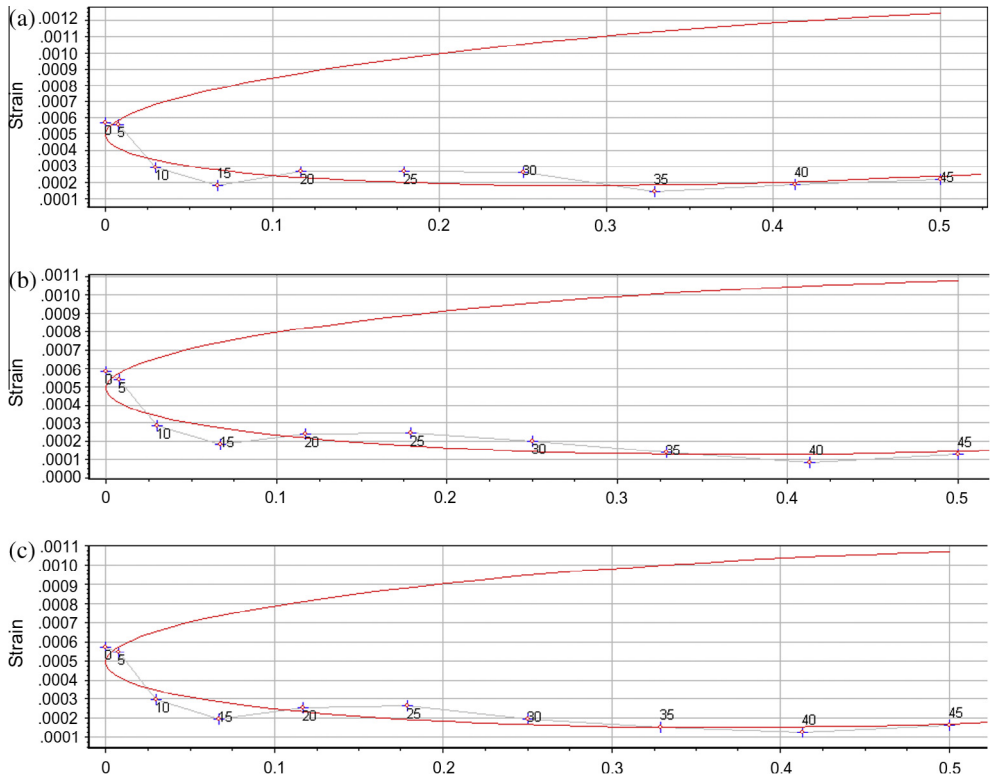

Fig. 13. Strain Vs $Sin^2 \psi$ plots of residual stress measurement using various peak evaluation methods. $Sin^2 \psi$ is on the *X*-axis. (a) Sliding gravity method, (b) Gravity method, and (c) Pearson VII method.

in an inclined arrangement, which provided varied normal load. In the present work, the investigated parameter is shoulder penetration into the workpiece to cause proper softening and flow of material during the process. This parameter is referred to as plunge depth. It is generally understood that a plunge depth of 0–0.3 mm leads to an efficient FSW/FSP depending on the type of material to be processed. Two sets of experiments were carried out to optimize the plunge depth for AA 2024-T3 alloy in the present work. In the case of AA 2024-T3, an optimum plunge depth of 0.23 mm was obtained for a defect free process. Transverse cross section of the processed region at this plunge depth shows a defect free macrostructure with a less sharp boundary. However, the surface finish was not much good with significant flash formation associated with it. Reason for the higher plunge depth requirement could be related to the high strength of this particular alloy. As the plunge depth increased, heat input to the material increased, this in turn softened the material for a smoother flow from leading edge to the trailing edge. The higher plunge depth also caused significant thickness of the material to be removed from the top surface, leading to the formation of flash on the surface and a rougher surface finish. The macrograph of the processed regions in the case of very low plunge depth as well as very high plunge depths are shown in Fig. 14 for the first set of varying plunge depth experiment. First four images (a–d) correspond to very low plunge depths of 5.26, 5.32, 5.38 and 5.44 mm respectively. The remaining three images (e–g) correspond to higher plunge depths of 5.68, 5.74 and 5.78 mm respectively.

It can be seen that the defect area increased as the plunge depth increased from 5.26 to 5.32 mm. This is also the reason for the sudden drop in UTS value of the second sample as compared to first sample in the case of varying plunge depth experiment. However, the defect area reduced considerably beyond this plunge depth, as shown in Fig. 14e. It is to be noted that at higher plunge depths, which correspond to more than 0.15 mm of shoulder penetration into the material, defects are not present. This is particular to this high strength aluminium alloy, which needs higher plunge depth for proper softening of the material and effective filling of the pin hole as it traverses. The only case when defects are visible for higher penetration depths correspond to plunge of more than 0.3 mm for the image shown in Fig. 14f.

Varying RPM experiments were done with the optimum plunge depth of 0.23 mm. It is observed that as RPM increased UTS value reduced continuously, and at higher speeds UTS value was very low, owing to the nature of fully defective FSP. By keeping the plunge depth and traverse speed fixed and varying the RPM, the process pitch defined as the ratio of traverse speed to rotation speed, decreased considerably, implying that the amount of material moved per second decreases as we increase the RPM. Calculation for the amount of material moved can be done as follows: By considering the tool rotation speed in RPM as '*N*', the time required for one rotation in second is 60/*N*. Representing the tool traverse speed in mm/min as '*V*', tool traverse speed in mm/s is given as *V*/60. Then the displacement or the material moved per second will be *V*/*N*. In current study, for the varying RPM experiment, material moved as per this equation was calculated. The amount of material moved will be one-third of that at an RPM of 300 than it is at 900 RPM. Amount of material moved changes from 166 μm to 58 μm as we change the RPM from 300 to 900 while keeping the traverse speed constant at 50 mm/min and plunge depth as 0.23 mm. The amount of material removed decreases as the RPM increases, and hence the improper filling of the tool pin hole occurs leading to defective FSP at higher tool rotational rates. In general, as the RPM increases heat input into the material increases, and the material flow occurs much easily. However, in our case, for this high strength aluminium alloy 2024, the plunge depth/normal load requirement was comparatively higher, and hence the heat input requirement from the tool rotation speed was lesser. As a result, a lower RPM of 350 led to completely defect free FSP. Macrographs of the processed zone at higher RPM's are shown in Fig. 15.

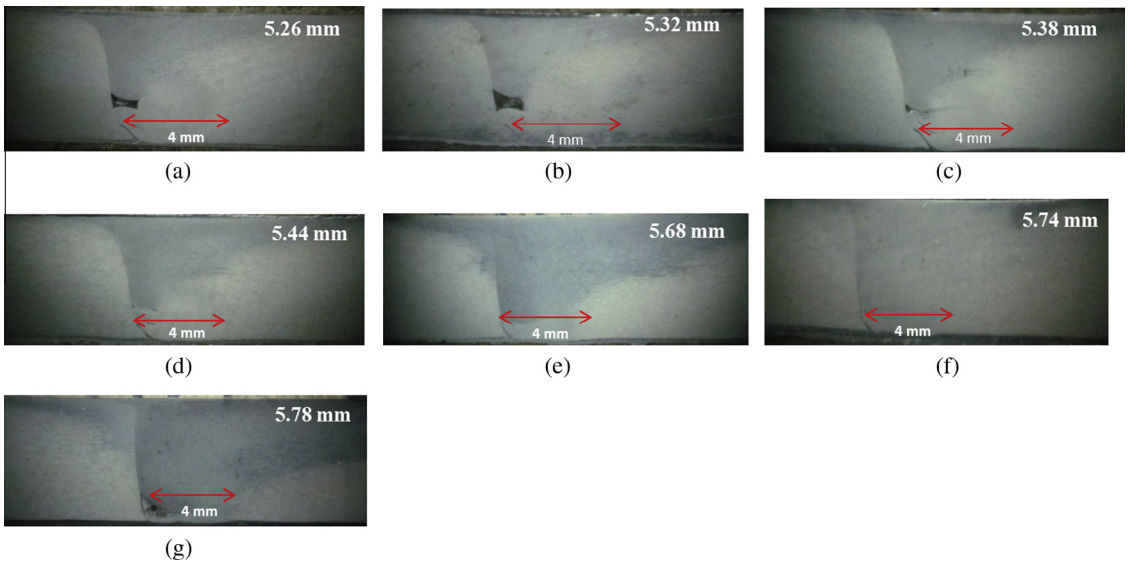

Fig. 14. Macrographs corresponding to different plunge depths. Plunge depth in 'mm' is highlighted at the top right corner of each figure.

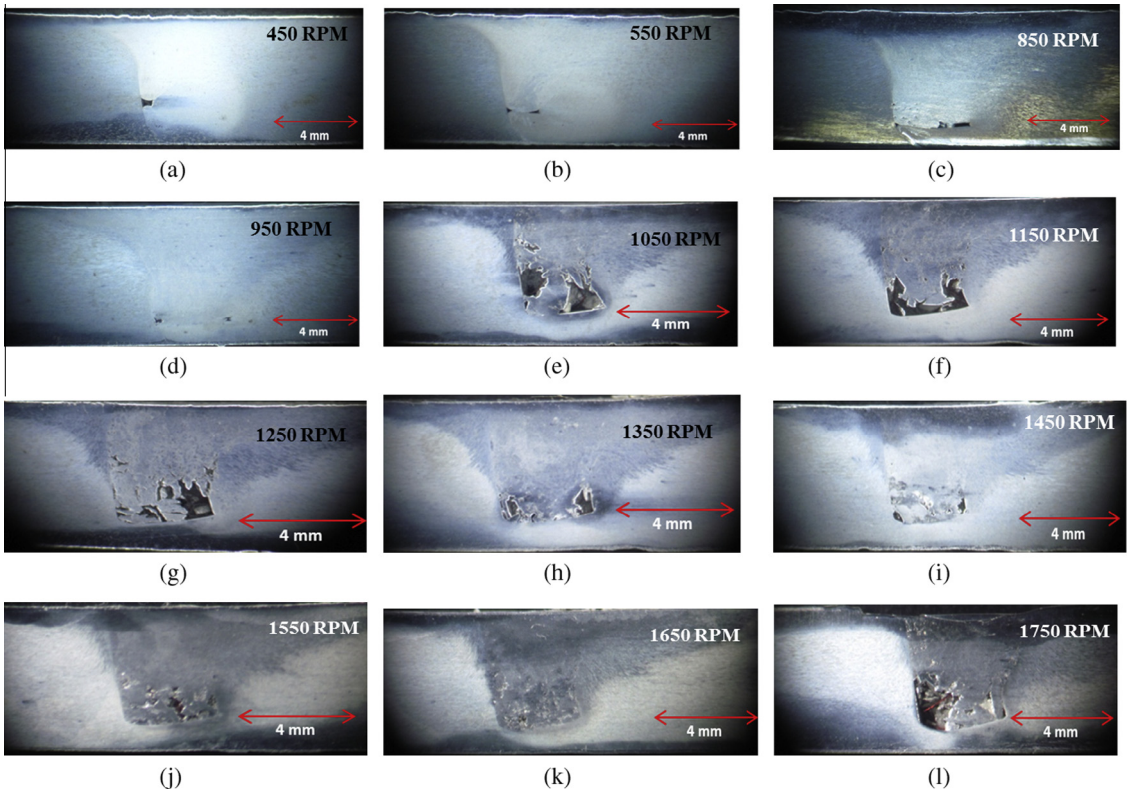

Fig. 15. Macrographs from varying RPM experiment. RPM is highlighted at the top right corner of each figure.

The macrographs in Fig. 15 correspond to the variations of RPM from 450 to 1750 with an interval of 100 RPM in most cases. The formation of defects were observed in all cases, and the description of the reasons of defect formation at higher tool rotational rates while keeping fixed traverse speed and plunge depth was described in the previous section.

In the current study, for a lower traverse speed such as 10 mm/min higher values of UTS and elongation was observed. The comparatively higher UTS and percentage elongation combination was observed for a traverse speed of 95 mm/min. Varying traverse speed experiment was conducted in two steps and is already detailed in the experimental section. This particular value of traverse speed 95 mm/min was a part of both set of experiments, and hence the results were reproducible in two cases. Amongst these two values of traverse speed, the higher value of 95 mm/min was selected in the present case. Traverse speed was fixed as 95 mm/min for the optimized RPM of 350 as per previous varying RPM experiments. FSP parameters obtained were the same as that used in a study by Staron et al. [14] for the residual stress measurement in the same alloy, except the plunge depth. Variation of

the process zone with the traverse speed is shown in Fig. 16. The figure shows macrographs taken at the transverse cross section of the processed samples for different traverse speeds.

It is to be noted that nature of the defects at a lower traverse speed and higher traverse speed are entirely different. At low traverse speeds the material flow is quite smooth. A sharp boundary with a small wormhole is observed as the traverse speed increases. At higher traverse speeds size of the wormhole is increased and it appears like two inter connected holes. The optimization of traverse speed is not well documented in the literature. However, from the present work it can be inferred that the traverse speed is also an important process parameter for an effective FSP. The most significant differences between the variation in traverse speed and RPM are the defect density and location of defect. In the case of varying traverse speed, the defect is only on one side in the processed zone at the advancing side. This can be completely avoided by doing multi-pass FSP with parallel passes on the advancing side.

4.2. Mechanical properties and residual stress

Mechanical properties of the processed materials are important as the objective of FSP is to produce materials with improved properties. Bulk mechanical properties will determine the service performance of the processed component. During the optimization stage of various processing parameters maximum value of Ultimate Tensile Strength (UTS) in MPa was lesser than that of the base metal. In the case of varying plunge depth experiments, the maximum observed value of UTS was approximately 320 MPa with the other two parameters fixed. For varying RPM experiment with the optimum plunge depth value the maximum value of UTS was approximately 310 MPa. With the optimum values of plunge depth and RPM the maximum UTS was approximately 375 MPa for a traverse speed of 95 mm/min. While FSP was done with optimum parameters strength obtained was significantly higher with a UTS value of 422 MPa. Theoretically, values of the last two should be the same, but the former being measured from the varying traverse speed experiment the effect of starting and intermediate traverse speeds will affect the same. The value obtained in present study was higher than that published in previously carried out work on the same alloy [15], and at par with that reported in the work of Hu et al. [16] for the same alloy in O temper. Fractured specimens are shown in Fig. 17. Fracture occurred at the Heat Affected Zone (HAZ) of the processed sample, which shows limitation of FSP in heat treatable materials. Further, precipitate coarsening occurs at this region during FSP, and hence acts as the weakest region during mechanical testing. This was already reported in previous work of Biallas et al. [17] and Magnusson and Kallman [18]. This cannot be avoided in a single pass FSP because HAZ is always an inherent part of a single pass FSP. However, single pass FSP is of limited applicability and multiple pass FSP need to be done for the bulk production of ultrafine grained materials with improved properties. Weaker regions can be avoided in the consecutive passes and this issue can be avoided to a certain extent except at start and end of the process.

Micro tensile testing of the samples taken from the nugget zone of FSP samples showed maximum UTS of 1.3 times the base material strength which is approximately 600 MPa. Testing was done on many samples taken from the top, bottom and middle of the nugget zone of the FSP samples across the thickness. The higher strength is a combined result of the grain size strengthening, and extensive distribution of the Al_2CuMg precipitates on the grain boundaries. The distribution can be visualized in the Phase Identification Map (PIM) shown in Fig. 18. It shows PIM from the EBSD scanning done on the nugget zone of optimum FSP sample. The scan was done with two phase inputs Aluminium and Al_2CuMg, both of which have different crystal structures. From PIM it can be observed that large distributions of Al_2CuMg precipitates are at the grain boundaries. This might contribute to the increase in strength.

In the current study of FSP on this alloy, no special cooling method was involved, and normal cooling of specimens after the processing is usually very slow. Fig. 18 also indicates the

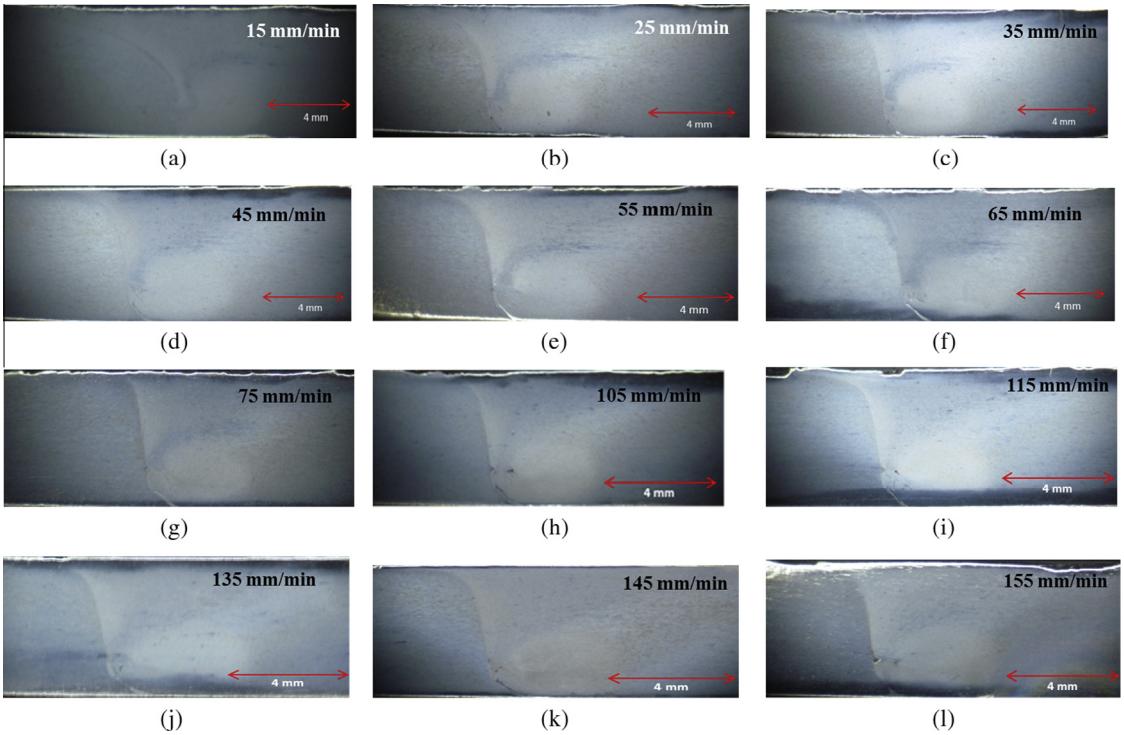

Fig. 16. Macrographs taken at different traverse speeds. Tool traverse speed in 'mm/min' is highlighted at the top right corner of each figure.

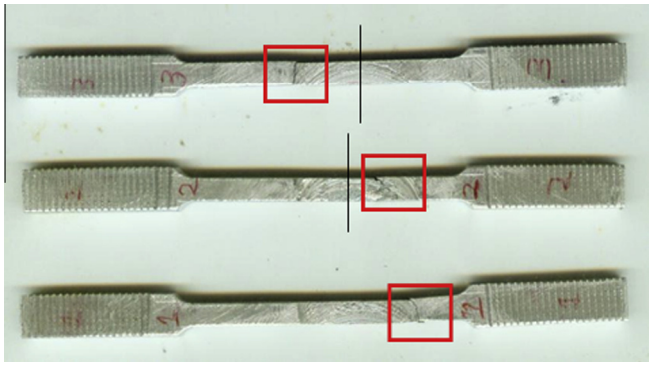

Fig. 17. Fractured tensile specimens. Fracture locations of tensile specimens are shown in the red box. Center of the processed zone is marked as the black vertical line. (For interpretation of the references to colour in this figure legend, the reader is referred to the web version of this article.)

occurrence of both heterogeneous and homogeneous nucleation during the processing, as precipitates are observed at the grain boundaries as well as at the grain interiors. In general, the preferred nucleation sites for heterogeneous nucleation are grain boundaries; the same being a rapid process precipitates grows larger in size. In case of FSP, the workpiece is heated nearly to its solution heat treatment temperature and cools down slowly. Hence, when it cools slowly the points of easy nucleation are the grain boundaries below the solvus line, and hence precipitation at grain boundaries is much higher. So, comparing with the base metal a much finer grain size along with the distribution of the precipitates at the grain boundaries is observed for optimum FSP sample. This will provide the grain boundary strengthening as well as precipitation hardening, and is responsible for the strength increase in processed materials.

It is well known that the residual stresses on the processed surface are also a determining factor for commercial usage of a process like FSP. Residual stress measurements reveal that all the stress values are tensile in nature. For the normal components, both the longitudinal and transverse stresses were less than 30 MPa in all the cases when various peak selection methods were used. The base material yield strength was approximately ~300 MPa, and hence the values of residual stress obtained with the optimum parameter FSP lies within the safe range for the aluminium alloy 2024-T3. Reason for the less value of residual stress is attributed to the solid state nature of FSP. The observed results confirm that temperature generated is below 550 °C during FSP. Otherwise, at a temperature of around 550 °C, incipient melting is expected for this alloy 2024 and this would have increased the tensile residual stress values. The observed residual stress values were in good agreement with those from the work of Prime et al. [19], which was for FSW done on 25.4 mm thick plates of 2024-T351 and 7050-T7451. One of the reasons being stated for the low residual stress in their work was the optimized weld they made. In present study, optimization was done through a systematic procedure and hence the peak tensile stress value was much lower than that reported in their work. We obtained residual stresses in the range of 10% of the yield strength of the material, whereas the value obtained was 15–20% in their work.

4.3. Microstructural observations of the optimum FSP sample

Microstructural features of the base metal and optimally processed FSP sample are shown in Fig. 19. Microstructure of the base material is shown in Fig. 19a, which represents the typical rolling microstructure with grains oriented along the rolling direction and precipitates distributed at the grain boundary as well as grain interiors. Microstructure of the FSP sample is shown in Fig. 19b, for the advancing side that was taken exactly at the middle of the thickness. It shows the boundary between nugget zone and TMAZ. It can be observed that the base metal is almost unaffected after FSP. Microstructure at the middle and top of the nugget zone is shown in Fig. 19c and d respectively.

It is to be noted that in these regions average grain size is 4–5 μm. However, volume fraction of precipitates are higher in the top of the nugget zone than in the middle, due to the relatively higher temperature generated at the top resulting from friction between the tool shoulder and workpiece. Higher thermal conductivity is one of the main reasons for uniform grain size across the thickness for materials like aluminium and copper, whereas the grain size variation across the thickness is significant for materials like titanium [20]. In case of materials like titanium and its alloys, the heat generated remains in the processed zone for larger time due to its low thermal conductivity, whereas for materials like aluminium alloys heat from the workpiece is transferred to the tool from the top and to backing plate from the bottom. In current

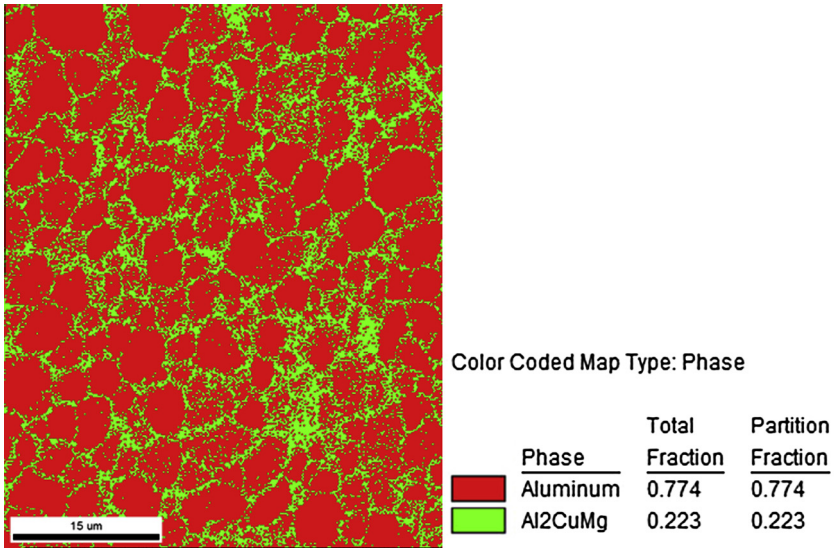

Fig. 18. Phase identification map for the nugget zone of optimum processed AA 2024 alloy.

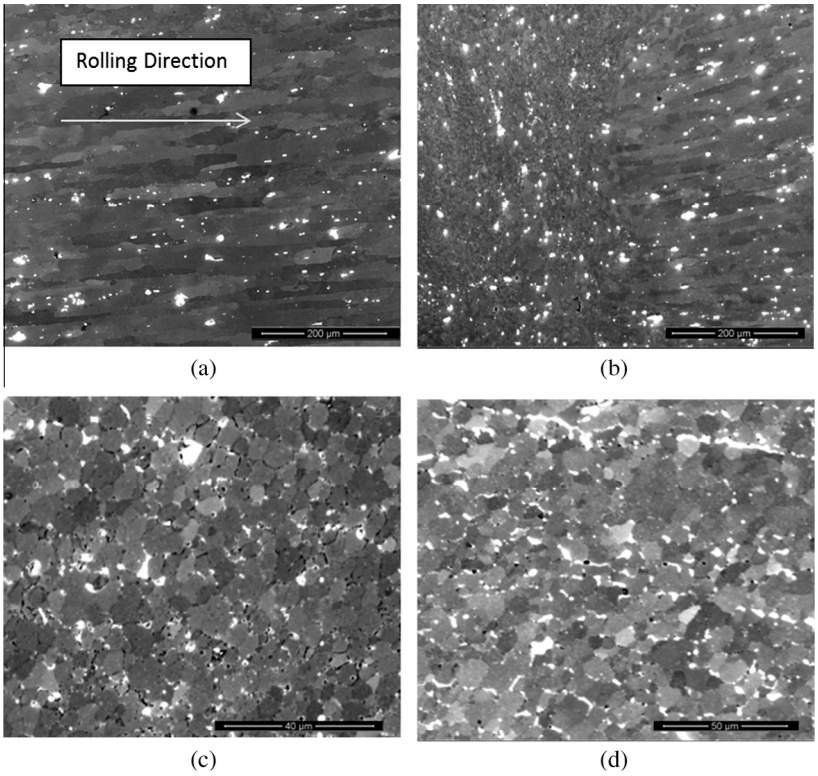

Fig. 19. SEM Images of the base metal and optimally processed FSP samples of AA 2024-T3. (a) Base metal, (b) advancing side, (c) middle of nugget zone, and (d) top of nugget zone.

study, the tool traverse speed used was 95 mm/min and this allowed faster cooling rates during FSP. Grain structure is equi-axed with an average grain size of 3–4 μm in the nugget zone of FSP samples. The equi-axed grain structure formation is due to the dissolution and a faster re-precipitation of Al_2CuMg precipitates in this alloy, which may not be possible for the case of a strain hardenable alloy. Faster cooling rates during FSP provides re-precipitation of the second phase particles and their uniform distribution along the grain boundaries. This does not allow further growth of grains even though the temperature generated during FSP is significantly higher for the abnormal grain growth to occur. The typical onion ring structure is also not evident in the nugget zone for the FSP done with optimum parameters for this alloy.

5. Conclusions

A bottom-up approach has been attempted to optimize the processing parameters with some fixed parameters and boundary conditions for a heat treatable aluminium alloy 2024 during FSP. Tensile testing was carried out to measure the mechanical properties of the processed samples. Average residual stress on the processed surface was measured using X-ray diffraction, and detailed microstructural characterization was done using optical microscopy, Scanning Electron Microscopy (SEM) and electron back scattered diffraction (EBSD). Major conclusions from the study are as follows:

(1) A proper combination of the three major processing parameters can lead to a completely defect free FSP with a less sharp boundary at the advancing side. The bottom-up approach applied here is a useful method in optimizing the processing parameters experimentally. Associated with the complex thermo-mechanical interactions and due to precipitation hardening response of the alloy 2024, analytical optimization of the processing parameters is not reliable and always gives rise to erroneous values. Hence, the bottom-up approach proposed in this investigation can be effectively used for optimizing the process parameters for this and other heat treatable alloys.
(2) The ultimate tensile strength value obtained is higher than in any of the published literature. Fracture location during the bulk tensile testing was the HAZ on advancing and retreating sides of the specimen where coarsening of the precipitates occur during the thermal cycle of FSP, which is the weakest zone in FSP sample.
(3) Micro tensile testing done on the nugget zone of the processed samples shows an ultimate strength of ~600 MPa, and the results were reproducible for a material with base metal strength of 450 MPa. Ductility in the processed zone was also the same as the base metal ductility. Thus proper combination of strength of ductility was obtained with FSP, which is not possible by other SPD techniques.
(4) Measured values of average longitudinal residual stress at the surface of optimum FSP samples were tensile in nature with a magnitude of less than 30 MPa, which is much lesser than the base metal yield strength of ~300 MPa. Hence, it is confirmed that FSP with optimal combination of parameters retains very less residual stress on the surface of processed components.
(5) Precipitation mechanisms during the thermal cycles associated with FSP were responsible for corresponding strength increase during the micro-tensile testing of FSP samples.

Acknowledgements

Authors would like to thank Department of Science and Technology (DST), Ministry of Human Resources Development

(MHRD), India. We would also like to thank Institute X-ray facility and Advanced Facility for Microscopy and Microanalysis (AFMM) at Indian Institute of Science, Bangalore for providing the facilities.

References

[1] Mishra RS, Mahoney MW, McFadden SX, Mara NA, Mukherjee AK. High strain rate superplasticity in a friction stir processed 7075 Al alloy. Scripta Mater 2000;42:163–8.
[2] Kim YG, Fujii H, Tsumura T, Komazaki T, Nakata K. Three defect types in friction stir welding of aluminium die casting alloy. Mater Sci Eng, A 2006;415:250–4.
[3] Aydin H, Bayram A, Uguz A, Akay KS. Tensile properties of friction stir welded joints of 2024 aluminium alloys in different heat treated state. Mater Des 2009;30:2211–21.
[4] Genevois C, Deschamps A, Vacher P. Comparative study on local and global properties of 2024 T351, 2024 T6 and 5251 O friction stir welds. Mater Sci Eng, A 2006;415:162–70.
[5] Jones MJ, Heurtier P, Desrayaud C, Montheillet F, Allehaux D, Driver JH. Correlation between microstructure and microhardness in a friction stir welded 2024 aluminium alloy. Scripta Mater 2005;52:693–7.
[6] Lakshminarayanan AK, Balasubramanian V. Process parameters optimization for friction stir welding of RDE-40 aluminium alloy using Taguchi technique. Trans Nonferrous Met Soc China 2008;18(3):548–54.
[7] Jayaraman M, Sivasubramanian R, Balasubramanian V. Optimization of process parameters for friction stir welding of cast aluminium alloy A319 by Taguchi method. J Sci Ind Res 2009;68(1):36–43.
[8] Fratini L, Corona V. Friction stir welding lap joint resistance optimization through gradient techniques. J Manuf Sci Eng – Trans ASME 2007;129(6):985–90.
[9] Okuyucu H, Kurt A, Arcaklioglu E. Artificial neural network application to the friction-stir welding of aluminium plates. Mater Des 2007;28(1):78–84.
[10] Diffract Plus, Leptos User Manual, DOC-M88-EXX104 V7 – December 2009, Bruker AXS GmbH.
[11] Corona A, Marchesi M, Martini C, Ridella S. Minimizing multimodal function of continuous variables with the simulated annealing algorithm. ACM TOMS 1987;13:262.
[12] Zhou C, Yang X, Luan G. Effect of root flaws on the fatigue property of friction stir welds in 2024-T3 aluminium alloys. Mater Sci Eng, A 2006;418:155–60.
[13] Kumar K, Kailas SV. On the role of axial load and the effect of interface position on the tensile strength of a friction stir welded aluminium alloy. Mater Des 2008;29:791–7.
[14] Staron P, Kocak M, Williams S, Wescott A. Residual stress in friction stir-welded Al sheets. Physica B 2004;350:e491–3.
[15] Khodir SA, Shibayanagi T, Naka M. Microstructure and mechanical properties of friction stir welded AA 2024-T3 aluminium alloy. Mater Trans 2006;47:185–93.
[16] Hu Z, Yuan S, Wang X, Liu G, Huang Y. Effect of post-weld heat treatment on the microstructure and plastic deformation behavior of friction stir welded 2024. Mater Des 2011;32:5055–60.
[17] Biallas G, Braun R, Donne CD, Staniek G, Kaysser WA. Mechanical properties and corrosion behavior of friction stir welded 2024–T3. Proceedings of the First International Symposium on Friction Stir Welding, Paper No. S3–P3, CA, USA, TWI Ltd.; 1999.
[18] Magnusson L, Kallman L. Mechanical properties of friction stir welds in thin sheet of aluminium 2024, 6013 and 7475. Proceedings of the Second International Symposium on Friction Stir Welding, Paper No. S2–P3, Gothenburg, Sweden, TWI Ltd. and IVF; 2000.
[19] Prime MB, Herold TG, Baumann JA, Lederich RJ, Bowden DM, Sebring RJ. Residual stress measurements in a thick, dissimilar aluminum alloy friction stir weld. Acta Mater 2006;54:4013–21.
[20] Edwards PD. Friction stir welding of Ti–6Al–4V sheet and plate for aerospace structures. PhD Thesis, University of Washington; 2010. p. 172–82.